Journal of Power Sources 251 (2014) 113–121

Contents lists available at ScienceDirect

Journal of Power Sources

journal homepage: www.elsevier.com/locate/jpowsour

Methanol synthesis from CO_2 hydrogenation over La–M–Cu–Zn–O (M = Y, Ce, Mg, Zr) catalysts derived from perovskite-type precursors

Haijuan Zhan [a,b], Feng Li [a], Peng Gao [a,b], Ning Zhao [a,*], Fukui Xiao [a], Wei Wei [a,c,*], Liangshu Zhong [d], Yuhan Sun [a,d,*]

[a] State Key Laboratory of Coal Conversion, Institute of Coal Chemistry, Chinese Academy of Sciences, South Taoyuan Road 27#, Taiyuan 030001, People's Republic of China
[b] University of the Chinese Academy of Sciences, Beijing 100049, People's Republic of China
[c] Center for Greenhouse Gas and Environmental Engineering, Shanghai Advanced Research Institute, Chinese Academy of Sciences, Shanghai 201203, People's Republic of China
[d] CAS Key Laboratory of Low-Carbon Conversion Science and Engineering, Shanghai Advanced Research Institute, Chinese Academy of Sciences, Shanghai 201203, People's Republic of China

HIGHLIGHTS

- La_2CuO_4 perovskite catalysts are prepared and tested.
- The promoter Y, Ce, Mg, Zr can improve the performance of perovskite catalysts.
- The perovskite catalysts show high selectivity for methanol.
- The conversion of CO_2 depends on the surface area of metallic Cu.

GRAPHICAL ABSTRACT

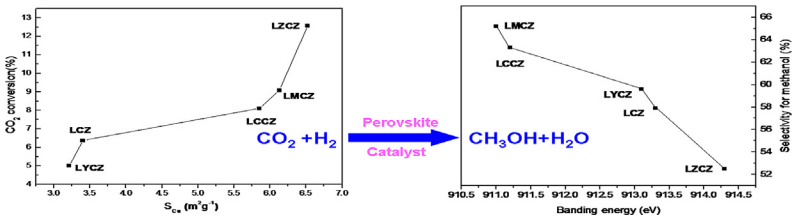

ARTICLE INFO

Article history:
Received 5 August 2013
Received in revised form
15 November 2013
Accepted 17 November 2013
Available online 26 November 2013

Keywords:
Perovskite
Carbon dioxide hydrogenation
Methanol
Sol–gel method

ABSTRACT

A series of La–M–Cu–Zn–O (M = Y, Ce, Mg, Zr) based perovskite-type catalysts are prepared by sol–gel method and characterized by XRD, BET, TPR, N_2O-adsorption, XPS and TPD techniques. The results indicate that all the catalysts exhibit La_2CuO_4 perovskite structure. The addition of Ce, Mg and Zr lead to smaller particles, lower reduction temperature, higher Cu dispersion, larger amount of hydrogen desorption at low temperature and more amount of basic sites. However, Y has less affects on the physicochemical properties. The catalysts derived from perovskite-type precursors show high selectivity for methanol, which is correlated with the $Cu^{\alpha+}$ species that exists in the reduced catalysts. More exposed Cu surface area is favorable for high CO_2 conversion.

1. Introduction

Carbon dioxide emissions from fossil fuels combustion and other human activity are considered as the main causes for global warming. Various strategies have been developed and implemented to reduce the carbon dioxide emissions [1–4]. As carbon dioxide is also a renewable, non-toxic and cheap feedstock for many chemical processes, the chemical conversion of CO_2 into value-added chemicals and fuels is very attractive and has been

* Corresponding authors. State Key Laboratory of Coal Conversion, Institute of Coal Chemistry, Chinese Academy of Sciences, South Taoyuan Road 27#, Taiyuan 030001, People's Republic of China. Tel.: +86 0351 4049612; fax: +86 0351 4041153.
E-mail addresses: zhaoning@sxicc.ac.cn (N. Zhao), weiwei@sari.ac.cn (W. Wei), yhsun@sxicc.ac.cn (Y. Sun).

0378-7753/$ – see front matter © 2013 Elsevier B.V. All rights reserved.
http://dx.doi.org/10.1016/j.jpowsour.2013.11.037

recognized as one of the most effective and economical ways to fix and utilize large amount of CO_2. CO_2 hydrogenation to methanol is an important process that offers challenging opportunities for sustainable development in energy and environment since methanol can be used as solvent, alternative fuel, and feedstock in the chemical industry [5]. Based on the great significance of methanol synthesis from CO_2 hydrogenation, the concept of "methanol economy" was also proposed [6].

Various catalytic systems have been investigated for CO_2 hydrogenation to methanol. Traditional Cu/ZnO catalysts derived from co-precipitation method are considered to be the most effective catalyst that has been studied for many years [7,8]. However, several important problems still remain opened, such as the working oxidation of copper and the reaction mechanism [9]. In addition, the low activity and stability of catalysts, which are partly attributed to Cu sintering accelerated by the presence of the byproduct, water vapor, create major barriers for practical application [10]. In order to improve the performance of the catalytic system, many promoters such as Al, Mn, Zr, Cr, Ga, B and rare earth metals have been studied [7,10–16]. It is found that the catalysts with higher Cu dispersion, easier reduction property and better adsorption properties for relative gases could achieve better catalytic performance for methanol synthesis [10].

Recently, much attention has been paid to perovskite-type oxides as catalysts due to their high activity and thermal stability. With the general formula of ABO_3 (A-site is a larger rare earth and/or alkaline earth cation and B-site is a smaller transition metal cation), the high dispersion of "metal-on-oxide" catalysts can be realized by reduction of perovskite-type precursors [15]. The metallic elements are stable in the perovskite structure when the radii meet the tolerance factor $t = (r_A + r_B)/2(r_B + r_O)$ $(0.75 < t < 1)$, so it is possible to prepare multi-component perovskite-oxides by partial substitution of A-site and/or B-site cations. In such a structure, the A-site keeps the structure and the B-site provides the catalytic activity site. B-site cations could be reduced to well dispersed metallic species supported on the A-site cations oxide, which leads to ideal catalyst precursors for many reactions that involve metal as active sites [17]. With this structural characteristic, the well-dispersion of the active sites of the catalyst can be obtained. Besides, perovskite-type A_2BO_4 mixed oxides with the K_2NiF_4 structure, consisting of alternating layers of ABO_3 perovskite and AO rock salt, have also been studied [18] which exhibit variable oxygen stoichiometry. Therefore, the replacement of A-site and/or B-site cations by other metal cations often results in the formation of crystal microstrain and adjustable activity [19]. For example, the La_2CuO_4 nanofiber was used for methanol reforming to CO_2 and H_2 which showed excellent performance [20]. The partial substitution of Co by Cu in the $LaCoO_3$ structure favored the CO hydrogenation to higher alcohols [21], and partial substituting of La at the A-site by Sr in La–Ni–Co–O or La–Co–O perovskite-type oxide exhibited promising activity and high stability for reforming of CH_4 with CO_2 [22,23]. However, little work on the application of Cu-based perovskite-type oxides for CO_2 hydrogenation has been investigated. In the present work, a series of La–M–Cu–Zn–O (M = Y, Ce, Mg, Zr) based perovskite-type catalysts were prepared and tested for CO_2 hydrogenation to methanol, the influence of the fourth elements on the perovskite structure, the relationship between the physico-chemical property and the catalytic performance of as-prepared catalyst were discussed.

2. Experimental

2.1. Catalyst preparation

The La–M–Cu–Zn–O (M = Y, Ce, Mg, Zr) perovskite-type oxides were prepared by sol–gel method using citric acid as complexing agent. Adequate amounts of the precursor salts ($La(NO_3)_3 \cdot nH_2O$, La_2O_3>44%; $Y(NO_3)_3 \cdot 6H_2O$; $Cu(NO_3)_2 \cdot 3H_2O$; $ZrO(NO_3)_2 \cdot 2H_2O$; $Zn(NO_3)_2 \cdot 6H_2O$; $Ce(NO_3)_3 \cdot 6H_2O$; $Mg(NO_3)_2 \cdot 6H_2O$) along with citric acid were dissolved in deionized water at a molar ratio of 2:1 (metal cations:citric acid). The solution was heated to 353 K to remove the water, and then increased to 423 K for 4 h. The resulting powder was calcined under air at 673 K for 2 h and then at 1073 K for 4 h. $LaCu_{0.7}Zn_{0.3}O_x$, $La_{0.8}Y_{0.2}Cu_{0.7}Zn_{0.3}O_x$, $La_{0.8}Mg_{0.2}Cu_{0.7}Zn_{0.3}O_x$, $La_{0.8}Ce_{0.2}Cu_{0.7}Zn_{0.3}O_x$, and $La_{0.8}Zr_{0.2}Cu_{0.7}Zn_{0.3}O_x$ samples were prepared, of which the subscripts were the nominal composition. The catalysts were then denoted as LCZ-173, LYCZ-8273, LMCZ-8273, LCCZ-8273 and LZCZ-8273, respectively.

2.2. Characterization of catalysts

Powder X-ray diffraction (XRD) patterns were recorded on a Panalytica X'Pert Pro X-ray diffractometer with Cu Kα radiation. The data of 2θ from 10° to 90° were collected with a step size of 0.05°.

The surface area of samples was determined by N_2 adsorption-desorption at liquid nitrogen temperature 77.30 K, using a Micromeritics Tristar 3000 instrument. Sample degassing was carried out at 473 K prior to acquiring the adsorption isotherm. The special areas were calculated from the isotherm using the Brunauer–Emmett–Teller (BET) method.

The dispersion of Cu (D_{Cu}) and exposed Cu surface area (S_{Cu}) were determined by dissociative N_2O adsorption and carried out on a Micromeritics AutoChem 2920 instrument. The catalyst (0.15 g) was first reduced in 5% H_2/Ar mixture (30 mL min^{-1}) for 2 h at 623 K, and the amount of hydrogen consumption was denoted as *X*. Then, the reduced sample was cooled to 338 K and isothermally purged with Ar for 30 min, after which the sample was exposed to N_2O (85 mL min^{-1}) for 1 h to ensure complete oxidation of the metallic copper. The sample was then flushed with Ar to remove the N_2O and cooled to room temperature. Finally, a pulse of pure H_2 was passed over the catalyst at 623 K. The surface Cu_2O was reduced in the pulse of pure H_2, and the amount of consumed H_2 was denoted as *Y*. The dispersion of Cu and exposed Cu surface area of the catalyst were calculated by the equation (1) [24] and equation (3) [25]

$$D_{Cu} = \frac{2Y}{X} \times 100\% \quad (1)$$

$$n_{Cu} = 2Y \quad (2)$$

$$S_{Cu} = (n_{Cu} \times N)/\left(1.4 \times 10^{19} \times W\right)\left(m^2 g^{-1}\right) \quad (3)$$

where D_{Cu} is the dispersion of Cu, *W* is the weight of the reduced catalyst, S_{Cu} is the exposed copper surface area per gram catalyst, n_{Cu} is the molar number of copper, *N* is Avogadro's constant (6.02×10^{23} atoms mol^{-1}), and 1.4×10^{19} is the number of copper atoms per square meter [24,25].

The morphology of the samples was investigated using a FETXL30 S-FEG scanning electron microscope (SEM) with an accelerating voltage of 10.0 kV.

X-ray photoelectron spectroscopy (XPS) measurements were performed over a Kratos XSAM800 spectrometer equipped with Al Kα radiation (12 kV × 15 mA, $h\nu$ = 1486.6 eV) under ultrahigh vacuum (10^{-7} Pa). The binding energies were calibrated internally by adventitious carbon deposit C(1s) with E_b = 284.6 eV (accuracy within ±0.1 eV).

Temperature program reduction (TPR) was carried out in a U-tube quartz reactor. The sample (50 mg) was purged with Ar (30 mL min^{-1}) for 1 h at 423 K to remove physically adsorbed water and then reduced in the flow of 5 vol.% H_2 + Ar (30 mL min^{-1}) at a

heating rate of 5 K min^{-1} up to 873 K. A thermal conductivity detector (TCD) was used to monitor the consumption of H_2.

The adsorption property of H_2 for the studied sample was measured by H_2 temperature-programmed desorption (H_2-TPD). The catalyst was first reduced at 623 K in a H_2 flow of 30 mL min^{-1} for 2 h. After cooling to room temperature, the catalyst was saturated with pure H_2 (30 mL min^{-1}) at 318 K for 60 min and then flushed with an Ar flow (40 mL min^{-1}) to remove all physical adsorbed molecules. Afterward, the TPD experiment was started with a heating rate of 10 K min^{-1} under an Ar flow (40 mL min^{-1}), and the change of the hydrogen signal was monitored by a TCD and quantitatively calibrated by H_2 pulses.

The basicity of the catalyst was measured by CO_2 temperature-programmed desorption (CO_2-TPD) and was performed in the same way as that of H_2-TPD; the only difference was that the desorbed CO_2 was detected by a BALZER mass spectrometer. The CO_2 peak area was quantitatively calibrated by injecting CO_2 pulses.

2.3. Evaluation of catalysts

Activity measurements in the hydrogenation of CO_2 were carried out in a continuous-flow, high-pressure, fixed-bed reactor. Catalyst (2.0 g, 40–60 mesh) diluted with quartz sand (60 mesh) was placed in a stainless steel tube reactor. Prior to reaction, the catalyst was reduced in pure H_2 at a flow-rate of 80 mL min^{-1} under atmospheric pressure. The reduction temperature was programmed to increase from room temperature to 623 K and maintained at 623 K for 8 h. The reactor was then cooled to room temperature. After reduction, the activity of the catalyst sample in the CO_2 hydrogenation process was determined under reaction conditions of 523 K, 5.0 MPa, $n(H_2):n(CO_2) = 3:1$, GHSV = 3600 h^{-1}. The steady–state activity values were quoted as the average of two different analyses taken after 24 h on the stream operation. Gas products were quantitative analyzed on-line with a gas chromatograph equipped with a thermal conductivity detector (TCD, TDX-01 column) and a flame ionization detector (FID, Carbosieve column). The liquid of water and methanol were determined off-line by a Porapak Q column. The CO_2 conversion and the carbon-based selectivity for CH_3OH and CO were calculated by an internal normalization method. The space time yield (STY_{CH3OH}), which gives the amounts of CH_3OH produced per gram catalyst per hour, is defined as the equation (4):

$$STY_{CH_3OH} = \frac{W_T \times X(CH_3OH)}{t \times m} \quad (4)$$

where W_T is the total weight of the CH_3OH and H_2O product; X(CH_3OH) is the mass fraction of CH_3OH; t is the reaction time; m is the weight of the catalyst.

3. Results and discussion

3.1. Textural and structural properties of the prepared materials

The X-ray diffraction patterns of the perovskite-type catalysts are shown in Fig. 1. It can be seen that the orthorhombic perovskite structure (A_2BO_4) with high degree of crystallinity of the La_2CuO_4 (JCPDS # 82-2142) is the main phase for all samples. Moreover, two small peaks at $2\theta = 35.6°$ and 38.9° ascribed to the CuO phase (JCPDS # 89-5899) present in all samples. The weak peak at $2\theta = 36.3°$ attributed to the ZnO phase (JCPDS # 80-0075) appears in all samples except LMCZ-8273. Doping of different elements lead to different changes for each sample, e.g. for LCCZ-8273, new peaks assigned to Ce_7O_{12} (JCPDS # 89-8431) can be observed at $2\theta = 27.9°$, 32.4°, 46.4°. In addition, for LZCZ-8273, a diffraction peak appears at $2\theta = 28.6°$ which can be ascribed to pyrochlore $La_2Zr_2O_7$ (JCPDS # 71-2362). However, no new phases containing Mg and Y appear in the sample of LMCZ-8273 and LYCZ-8273 which might be due to the highly dispersion of Mg and Y.

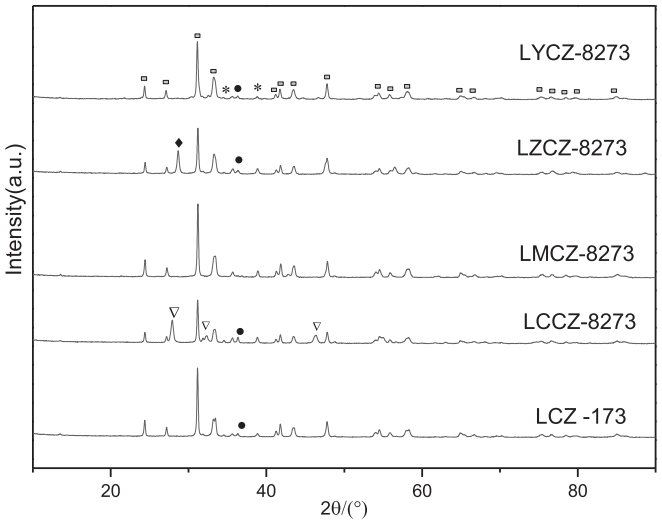

Fig. 1. XRD patterns of the perovskite-type catalysts: (□) La_2CuO_4; (*) CuO; (◆) $La_2Zr_2O_7$; (●) ZnO; (▽) Ce_7O_{12}.

With the formation of new phases for the samples of LCCZ-8273 and LZCZ-8273, the intensity of the La_2CuO_4 diffraction peak decreases and the LZCZ-8273 sample shows the weakest diffraction peak for La_2CuO_4. However, Mg seems to have a special effect on the structure since the peak of ZnO disappears for the LMCZ-8273 sample.

The crystallographic parameters of the prepared materials were calculated by employing least-squares refinement, assuming an orthorhombic crystal system for the samples, and the results are listed in Table 1. The introduction of the fourth component leads to a certain degree of changes of the lattice parameters. It can be seen that all the lattice parameters a, b and c were lower than those of LCZ-173 which can be attributed to the shrinkage of the La_2CuO_4 due to the introduction of the fourth elements. The mean grain size of La_2CuO_4 calculated by the Scherrer equation shows that the particles size of the La_2CuO_4 decreased remarkably upon introduction of Ce, Zr, Mg (except Y).

The physicochemical properties of the calcined catalysts are summarized in Table 2. The BET surface area for all calcined sample are rather low ($S_{BET} < 3$ m^2 g^{-1}) which is common for perovskite-type of materials [17]. It can be seen that the LZCZ-8273 has the highest specific surface area, while the LYCZ-8273 and the LCZ-173 have the lowest specific surface area. Moreover, the exposed Cu surface area and the Cu dispersion measured by N_2O adsorption have the same tendency. The LZCZ-8273 shows the highest Cu surface area (S_{Cu}) and the best dispersion of copper (D_{Cu}). The physicochemical properties of LYCZ-8273 are similar to that of the

Table 1
The lattice parameters of the perovskite-type catalysts.

Samples	Lattice parameters (Å)			Volume (Å^3)	Size of La_2CuO_4 crystallites (nm)
	a	*b*	*c*		
LCZ-173	5.365	5.409	13.170	383.8	95.6
LCCZ-8273	5.350	5.392	13.137	381.8	31.9
LMCZ-8273	5.352	5.400	13.157	380.6	22.5
LZCZ-8273	5.356	5.404	13.149	379.0	24.0
LYCZ-8273	5.359	5.363	13.127	377.3	84.5

Table 2
The physiochemical properties of the calcined perovskite-type catalysts.

Samples	S_{BET} ($m^2\ g^{-1}$)	Dispersion[a] (%)	S_{Cu} ($m^2\ g^{-1}$)
LCZ-173	0.7	5.3	3.4
LCCZ-8273	1.3	8.5	5.9
LMCZ-8273	1.2	8.5	6.2
LZCZ-8273	2.3	8.6	6.5
LYCZ-8273	0.7	4.5	3.2

[a] Calculated from N_2O dissociative adsorption.

LCZ-173 which indicates that the influence of the Y doping is negligible.

Generally, the replacement would be more likely to happen between the elements with similar radius, same valence state as well as same coordination numbers in the structure. As a result, it is easy for Ce to substitute La at the A site of the perovskite-type structure due to the similarity of the ionic radii of the two ions in 12-fold coordination (1.36 Å for La^{3+}, 1.34 Å for Ce^{3+} and 1.14 Å for Ce^{4+}) [26]. The replacement probably induces a structural disorder and thus hinders the crystallite growth, leading to higher specific surface area [27]. Because the characters of Y^{3+} are almost the same with La^{3+}, the Y substitution will also occur in the A-site which causes less change for the structure. As Zr is introduced, a pyrochlore structure ($La_2Zr_2O_7$) is formed and become clearly observed in the XRD pattern which may result in a good chemical stability for the system [28]. The $La_2Zr_2O_7$ is mainly composed of octahedral ZrO_6 as net structure with La^{3+} filled in the gap of the octahedral ZrO_6 [29]. As a result, the LZCZ-8273 possesses the largest specific surface area which provides space for better dispersion of copper species. Moreover, since it is very likely that Zr substitutes a part of La in the sample, it causes the decreasing of diffraction peak intensity of the La_2CuO_4. As for the LMCZ-8273, the valence state as well as the ionic radii for 6-coordination (0.72 Å for Mg^{2+}, 0.73 Å for Cu^{2+}, 0.74 Å for Zn^{2+}) of the Mg is the same as Cu and Zn [26]. Therefore, Mg might have stronger influence on the B-site of the perovskite-type oxide.

Fig. 2 shows the SEM images of different catalysts. It can be seen that all the samples are in the form of irregular particles. The quantitative analysis of obvious particle size for each catalyst was obtained with the program SmileView based on the SEM data (Fig. S1). The LCCZ-8273, LMCZ-8273, LZCZ-8273 have more small particles (about 0.4–0.6 μm) compared with the LCZ-173 and LYCZ-8273. The results indicate that the introduction of Ce, Mg or Zr favors the formation of small particles, while the Y may have less effect on the particle size, which is consistent with the results of the XRD analysis.

3.2. XPS investigations

The reduced perovskite-type catalysts are analyzed by XPS, and the binding energies (BE) of $Zn2p_{3/2}$, $La3d_{5/2}$ as well as the surface compositions of the catalysts are presented in Table 3. According to the literature, $La3d_{5/2}$ features in perovskite structure are located at 837.5 and 834.3 eV [27,30] which are close to the values of pure lanthana at 837.8 and 834.4 eV, indicating that lanthanum ions are present in the trivalent form. A slight shift in the $La3d_{5/2}$ binding energy is observed upon introduction of the fourth elements and the values are in the range of 837.86–838.01 eV and 834.06–834.36 eV, respectively. Small differences may relate to the changes in crystal structure and/or electronic structure. In addition, small changes are also observed for the binding energy of Zn at around 1021.7 eV for different samples.

All the BE of $Cu2p_{3/2}$ are located at ca 932.4 eV which is the characteristic peak of reduced Cu^+/Cu^0 species. Though the BE of the $Cu2p_{3/2}$ band in the Cu^0 (932.6 eV) and in Cu^+ (932.4 eV) are almost the same, they can be distinguished by the different kinetic energy of the Auger Cu LMM line position in metal (918.6 eV), Cu^+ (916.7 eV) or in Cu^{2+} (917.9 eV) [8]. The Auger electron spectroscopies of Cu LMM of reduced samples are shown in Fig. 3. It can be seen that a broad peak appears in the range of 915.0 eV–920.0 eV for all samples, which apparently cannot distinguish the Cu^+, Cu^{2+} and Cu^0. However, the peaks at around 918.6 eV are distinct for all samples. A new peak appears at around 911.2–914.3 eV, lower than that of Cu^+, is observed and can be defined as peak α, implying that

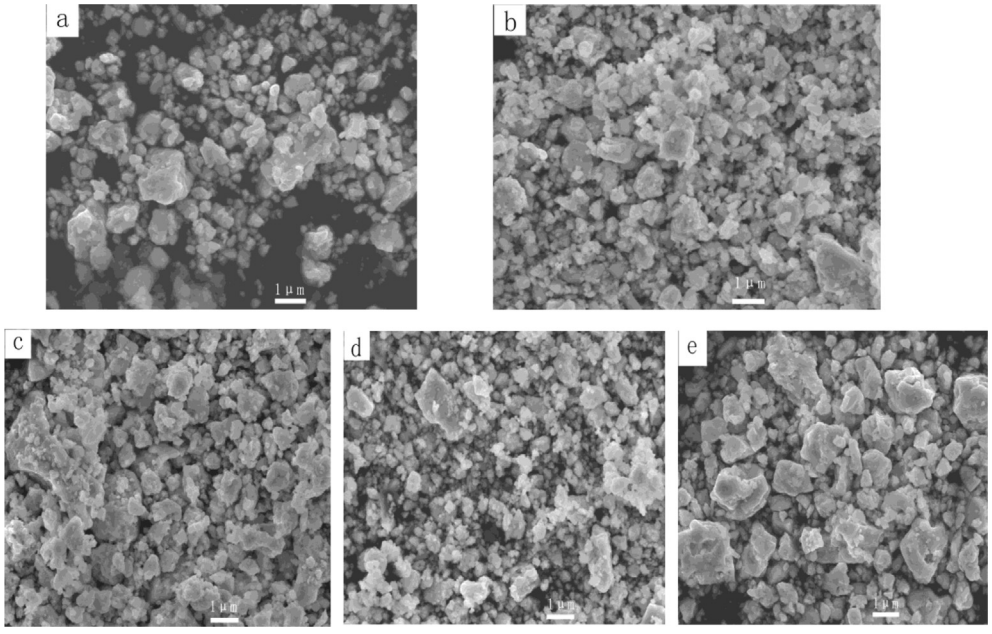

Fig. 2. SEM images of the catalysts: (a) LCZ-173, (b) LCCZ-8273, (c) LMCZ-8273, (d) LZCZ-8273, (e) LYCZ-8273.

Table 3
XPS parameters of the studied samples.

Samples	Binding energy (eV)			Relative surface concentration of metal (%)[a]			
	$La3d_{5/2}$		$Zn2p_{3/2}$	La	Cu	Zn	M
LCZ-173	837.89	834.15	1021.67	45.3(50)	39.9(35)	14.8(15)	–
LCCZ-8273	837.92	834.06	1021.71	45.3(40)	31.4(35)	15.6(15)	Ce: 7.7(10)
LMCZ-8273	837.87	834.36	1021.34	37.6(40)	38.9(35)	11.5(15)	Mg: 12.0(10)
LZCZ-8273	838.01	834.26	1021.78	50.5(40)	25.6(35)	14.5(15)	Zr: 9.4(10)
LYCZ-8273	837.86	834.23	1021.69	39.1(40)	40.9(35)	10.7(15)	Y: 9.3(10)

[a] Values in parentheses are nominal concentration normalized to the total metal content.

$Cu^{\alpha+}$ exists in the perovskite system. The specific Cu^0 and vague Cu^+ is important for the catalysts e.g. the presence of Cu^+ may accelerate the reduction of CO_2 to CO (RWGS) according to Fujita et al. [31]. While the $Cu^{\alpha+}$ (not Cu^{2+}, Cu^{1+}, Cu^0) plays an important role for the methanol synthesis from CO_2/H_2 as reported by F. Arena et al. [32,33].

The X-ray photoelectron spectroscopies of the fourth elements in the reduced samples are shown in Fig. 4. Seven binding energy peaks can be observed for the LCCZ-8273, i.e. 882.4/888.7/898.3 eV ascribed to Ce^{4+} $3d_{5/2}$, 907.4/916.2 eV assigned to Ce^{4+} $3d_{3/2}$, 884.5 eV attributed to Ce^{3+} $3d_{5/2}$ species and 900.6 eV ascribed to Ce^{3+} $3d_{3/2}$ [34], which suggests that both Ce^{3+} and Ce^{4+} exist in the LCCZ-8273 and the 4+ oxidation state is predominant. The result agrees with the XRD analysis. Since the highest valence state of Ce exists in the LCCZ-8273, it can be speculated that part of the electrons transformed from Ce to Cu in the perovskite structure. For the sample of LMCZ-8273, the BE of $Zn2p_{3/2}$ is much lower than that of LCZ-173, and the BE of Mg2p shifts from 49.8 eV in theory [35] to 49.2 eV (Fig. 3). Combining the analysis of XRD, it can be speculated that Mg and Zn species have strong interaction with each other or with other elements in the perovskite structure. For LZCZ-8273, the binding energy of 183.4 eV and 181.3 eV can be assigned to the $Zr3d_{2/5}$ and its satellite, which are very close to the value of that of $La_2Zr_2O_7$ [36]. It indicates that the Zr in the sample exists in the phase of $La_2Zr_2O_7$, which is consistent with the XRD analysis. For LYCZ-8273, the BE for $Y3d_{5/2}$ (BE = 156.7 eV) changes a little compared with that in theory (156.6 eV) [37].

The surface compositions of the nominal compositions of the catalysts are also listed in Table 3. It can be seen that the fourth element had different influences on the surface compositions. The enrichment of Cu and depletion of Zn and La occurred for the catalyst of LCZ, and this feature was kept when Mg and Y were introduced.

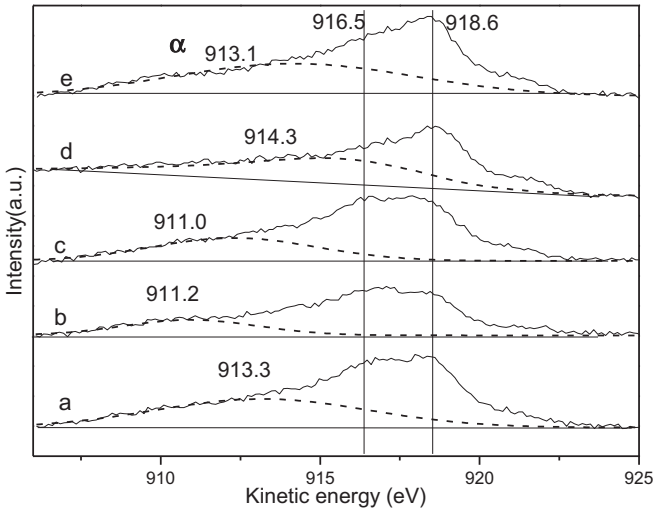

Fig. 3. Cu LMM Auger electron spectroscopy of (a) LCZ-173; (b) LCCZ-8273; (c) LMCZ-8273; (d) LZCZ-8273; (e) LYCZ-8273 samples after reduce.

3.3. The reducibility of the catalysts

In order to assess the reduction behavior of the catalysts, TPR measurements were carried out (Fig. 5). It can be seen that all samples exhibited a broad reduction peak in the temperature range of 503–630 K which can be attributed to the reduction of copper species. No other reduction peaks are observed. In order to have more insight into the TPR results, the profiles were deconvoluted into several Gaussian peaks. The low-temperature peak β may due to the reduction of dispersed copper species, and the peak γ at the high-temperature may be attributed to the reduction of bulk copper species. The peak α at even lower temperature can be ascribed to the well-dispersed copper species in the samples [38]. The peak positions and their contribution are summarized in Table 4. Obviously, compared with LCZ-173, the reduction temperature is lowered and the concentration of species which can be easily reduced increases for all the samples with the addition of the fourth element, indicating that the doped elements improve the reducibility of the sample. For the LCCZ-8273 sample, the peak α shifts to much lower temperature and the peak γ even disappears. For the sample of LZCZ-8273, three obvious reduction peaks are observed which is in accordance with the textural and structural properties of the largest specific surface area and well dispersion of the copper species. While LYCZ-8273 displays the higher reduction temperature originated from larger amount of bulk copper species due to the larger particles as illustrated by SEM and XRD. Y has poor influence on the perovskite structure which leads to fewer changes for the reduction property of the sample.

3.4. H_2-TPD

Table 5 shows the desorption temperature and H_2 desorption amount for each sample derived from H_2-TPD tests. It can be seen that the H_2 desorption occurs at a temperature of around 405 K and 700 K. The peak at about 405 K represents the desorption of atomic hydrogen on the surface of Cu site [39]. With the addition of the fourth element, the desorption peak at low temperature shifts to even lower temperature, and the amount of hydrogen desorbed increases compared with that of LCZ-173. The increasing trend of the amount of desorbed atomic hydrogen at low temperature is consistent with that of the reduction temperature of the peak α derived from TPR results which might because the lower the reduction temperature is, the more atomic hydrogen can be absorbed on the surface of Cu sites. It is worth stressing that only the H_2 desorbed at lower temperature is useful since the methanol synthesis from CO_2/H_2 often happens below 623 K. In other words, proper adsorption strength of atomic hydrogen is beneficial for the CO_2 hydrogenation to methanol [40].

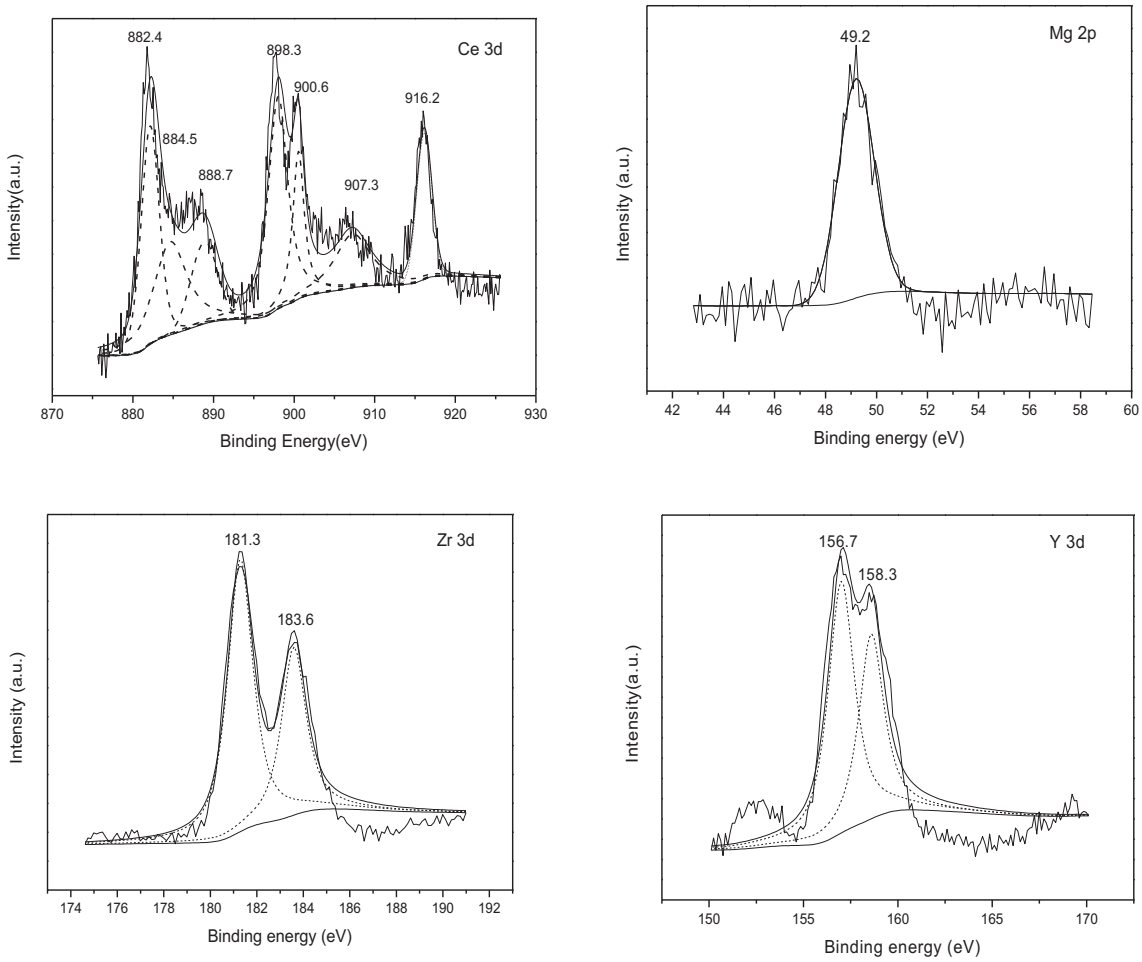

Fig. 4. The XPS spectra of Ce3d, Mg2p, Zr3d and Y3d.

The desorption peak which appeared at a high temperature can be ascribed to the strongly adsorbed hydrogen from the copper species in the bulk phase or on the ZnO phase. The site of the adsorption may be the Cu^{+}–O–Zn^{2+}. It was reported that the CuO and the ZnO can retain the hydrogen because hydrogen can transport from the surface copper to the bulk copper species or/and ZnO via spillover [39,41,42].

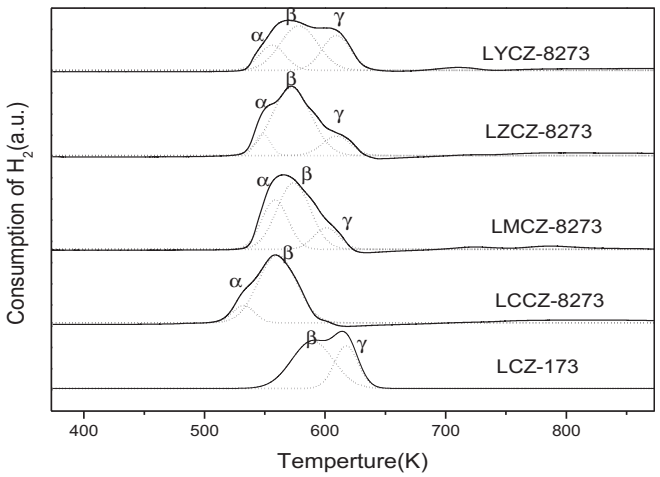

Fig. 5. The TPR profiles of the catalysts.

The amount of desorbed hydrogen from both low and high temperatures increases with the doping of the fourth elements which indicates that the modified samples could promote the hydrogen adsorption of the catalysts.

3.5. The surface basicity of the catalysts

Fig. 6 shows the CO_2 desorption profiles of the reduced catalysts, and the distribution of different adsorption sites are listed in Table 6. Two desorption peaks, the weak (at around 400 K) and the strong basic (at around 550 K) sites, are observed which might originate from the OH^{-} groups and the coordinatively unsaturated O^{2-} ions [43].

Obviously, the introduction of Ce, Zr and Mg improves the formation of both the weak basic sites and the strong basic sites. The addition of Ce and Zr lead to a considerable increasing of the strong basic sites which might associate with the higher net electronic of the perovskite structure that results in more low coordination oxygen atoms. The basicity of the mixed oxide increased through the formation of Ce^{4+}–O^{2-} and Zr^{4+}–O^{2-} acid–base pairs [44]. Upon addition of Y, a small amount of strong basic sites are found while the weak basic sites and the total basic sites decreased.

3.6. Catalytic performance

The catalytic performance for reduced perovskite-type catalysts are summarized in Table 7. It is found that the LZCZ-8273 shows the

Table 4
Center of reduction peaks and their contribution to the TPR pattern over the studied samples.

Sample	The peak position [temperature (K)] and concentration (%)[a]		
	Peak α	Peak β	Peak γ
LCZ-173	–	591(78.4)	618(21.6)
LCCZ-8273	495(12.8)	560(87.2)	–
LMCZ-8273	556(36.5)	573(44.4)	603(19.1)
LZCZ-8273	546(9.0)	573(75.5)	611(15.5)
LYCZ-8273	557(9.8)	577(76.8)	609(13.4)

[a] Values in parentheses are the contributions (%) of each species.

Table 5
The desorption temperature and the amount of desorbed H_2 for reduced catalysts.

Samples	T_1 (K)	H_2 desorption (μmol g^{-1})	T_2 (K)	H_2 desorption (μmol g^{-1})
LCZ-173	411	15.49	681	63.03
LCCZ-8273	408	21.03	696	184.50
LMCZ-8273	400	19.37	690	101.09
LZCZ-8273	403	19.41	716	102.62
LYCZ-8273	406	15.72	689	170.75

highest CO_2 conversion and the maximum yield of methanol despite the lowest selectivity among all the samples. The LMCZ-8273 shows the highest methanol selectivity and the LCCZ-8273 shows moderate CO_2 conversion and methanol selectivity. The lowest CO_2 conversion and less improvement for methanol selectivity are observed for LYCZ-8273.

The varying of the CO_2 conversion had the same tendency as the surface area of copper (Fig. 7), indicating more surface copper existing in the catalysts may lead to higher activity e.g. the copper species are the active sites for CO_2 hydrogenation to methanol [10,11,14,32,39]. Other phases affect the catalytic performance by influencing the dispersibility, reducibility, adsorbability of the copper species.

It is noteworthy that all catalysts show promising CH_3OH selectivity, especially for LMCZ-8273. The order of the selectivity to CH_3OH is as follows: LMCZ-8273 > LCCZ-8273 > LYCZ-8273 > LCZ-173 > LZCZ-8273. The relationship between CH_3OH selectivity and the binding energy of the Auger peaks (peak α) for all samples is

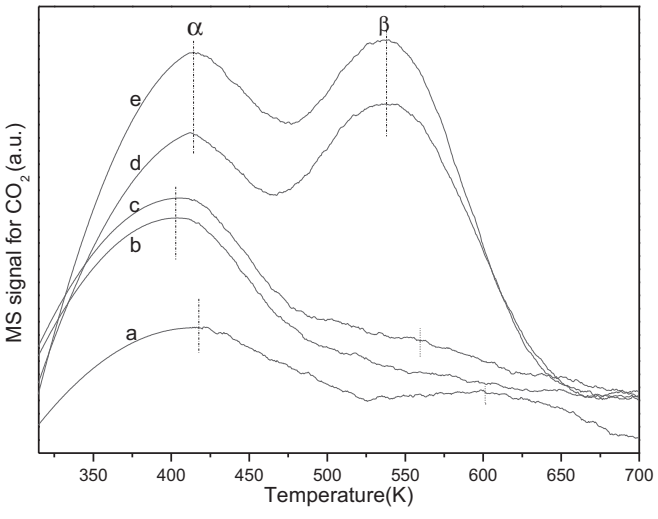

Fig. 6. CO_2–TPD curves of the catalysts. (a) LYCZ-8273; (b) LCZ-173; (c) LMCZ-8273; (d) LZCZ-8273; (e) LCCZ-8273.

Table 6
The basicity calculated from CO_2–TPD data.

Samples	Adsorption type and distribution based in CO_2–TPD data[a]		
	Peak α	Peak β	Total
LCZ-173	1.00	0	1.00
LCCZ-8273	1.51	1.60	3.11
LMCZ-8273	1.12	0.28	1.40
LZCZ-8273	1.27	1.39	2.66
LYCZ-8273	0.59	0.32	0.91

[a] The amount of basicity of LCZ-173 was assigned as 1.0 and compared with other samples.

Table 7
The catalytic performance for methanol synthesis from CO_2 hydrogenation over the reduced catalysts.

Samples	CO_2 conversion (%)	Selectivity (C-mol%)			CH_3OH yield (g $gcat^{-1}$ h^{-1})	TOF(Cu) × 10^3 (s^{-1})
		CH_3OH	CO	CH_x		
LCZ-173	6.4	57.9	39.5	2.5	0.05	65.1
LCCZ-8273	8.1	63.3	34.9	1.7	0.08	48.9
LMCZ-8273	9.1	65.2	33.0	1.8	0.09	52.0
LZCZ-8273	12.6	52.5	46.0	1.4	0.10	68.0
LYCZ-8273	5.0	59.6	37.0	3.5	0.04	55.7

Reaction conditions: $n(H_2)/n(CO_2) = 3:1$, $T = 523$ K, $P = 5.0$ MPa, GHSV = 3600 h^{-1}.

shown in Fig. 8. It can be seen that as the binding energy of the peak α shifts to lower value, higher CH3OH selectivity is observed. Since the presence of the Cu^+ accelerates the reduction of CO_2 to CO (RWGS), it can be derived that the farther away from 916.6 eV (the binding energy of Cu^+ in Cu LMM) for the peak α, the higher the CH_3OH selectivity can be obtained, suggesting that the $Cu^{\alpha+}$ had a strong effect on the selectivity for methanol. As discussed above, doping of Mg leads to the proper oxide state of copper that results in the best selectivity for methanol. For LCCZ-8273 and LYCZ-8273, Ce and Y substitute La in the A-site with the same charge (3+) and similar ionic radius which produces more defects in the perovskite structure that cause the special oxide state for copper species. With the special structure of La_2CuO_4 perovskite, the high dispersed copper species can be realized and stronger physical and electric interaction between the copper and other metal oxides can be obtained which may lead to the formation and stabilization of the copper species with special valence [45]. However, for the

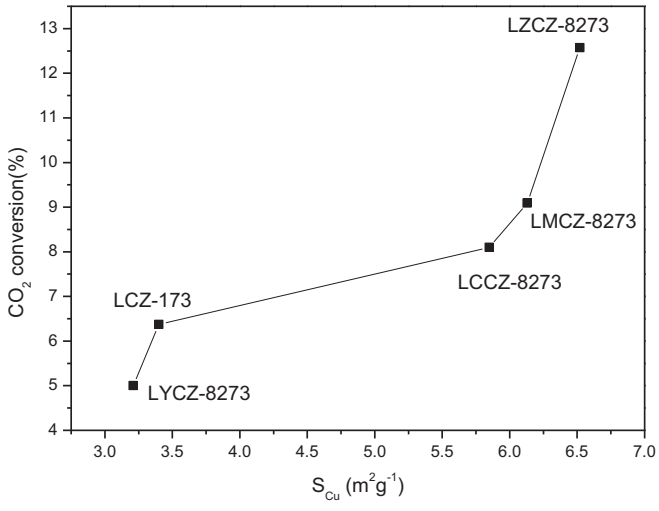

Fig. 7. The relationship between copper surface area and CO_2 conversion.

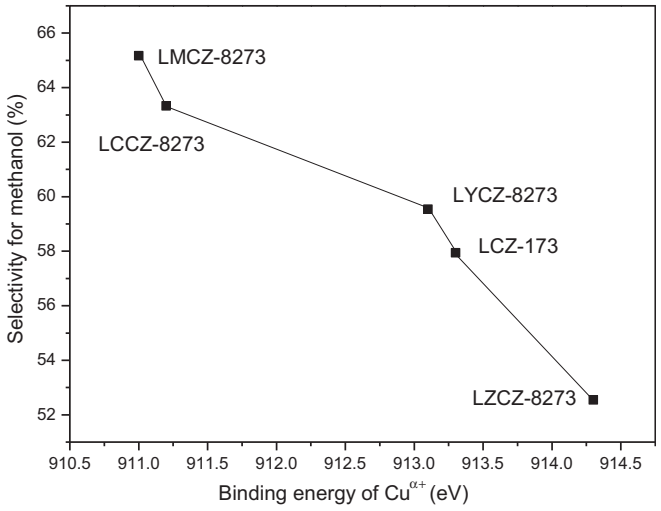

Fig. 8. The relationship between methanol selectivity to methanol and binding energy of $Cu^{\alpha+}$.

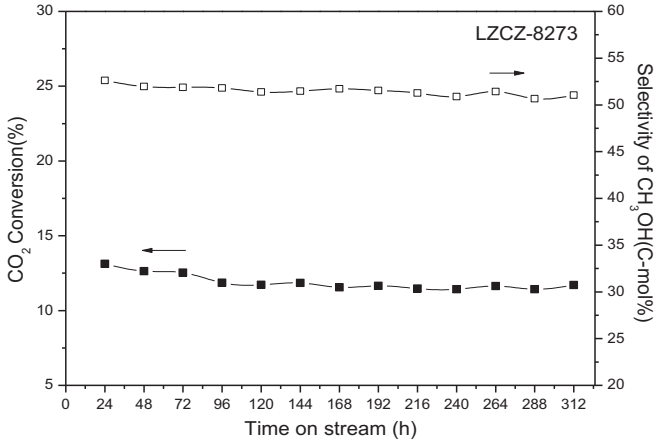

Fig. 9. The long-term stability test of LZCZ-8273 catalyst for 312 h. Reaction conditions: $n(H_2)/n(CO_2) = 3{:}1$, $T = 523$ K, $P = 5.0$ MPa, GHSV = 3600 h^{-1}.

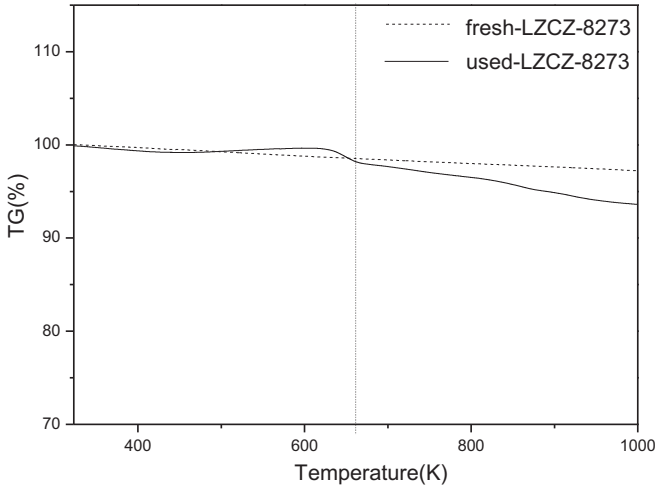

Fig. 10. TG curves for the LZCZ-8273 sample.

LZCZ-8273, the formation of lanthanum zirconium pyrochlore has little influence on the perovskite structure but a great influence on the content of La_2CuO_4 perovskite which may lead to the lowest selectivity of methanol.

The turnover frequency (TOF), which represents the number of CO_2 molecules hydrogenated in a unit site per second (s^{-1}), is calculated from the exposed copper surface area for the perovskite-type catalysts (Table 7). The TOF values of the perovskite-type catalysts were very high compared with other systems [11,34], indicating the better efficiency for copper atoms on perovskite-type catalysts.

The long-term reaction results are showed in Fig. 9. It can be seen that the LZCZ-8273 sample is stable after 312 h of running. During the whole test time, the catalyst showed a stable yield of methanol without obvious deactivation. Since the decreasing of CO_2 conversion could be caused by carbon deposition, the thermogravimetric method was carried out to study the carbon deposition over LZCZ-8273 (Fig. 10). It can be seen that there is a little weight losses at the temperature higher than 660 K that may be associated to the decomposition of coke and/or carbon filaments present on the catalyst surface [46]. The carbon element analyses revealed that the fresh and the used catalyst present the carbon content of 0.18% and 1.51%, respectively.

4. Conclusions

A series of La–M–Cu–Zn–O (M = Y, Ce, Mg, Zr) catalysts derived from perovskite-type precursors were prepared via sol–gel method. The results show that all the catalysts are La_2CuO_4 (A_2BO_4) perovskite structure. With the addition of Ce, Mg and Zr, catalysts with smaller particles, lower reduction temperature, higher Cu dispersion, larger amount of hydrogen desorption at low temperature as well as higher concentration of basic sites are obtained. Such perovskite catalysts also provide regular dispersion and special oxide state for copper species after reduction, which lead to improve methanol selectivity. The excellent methanol selectivity originates from the special copper valence which presents in the perovskite structure after reduction, the CO_2 conversion is in correlation with the surface area of metallic copper which in the reduced catalyst.

Acknowledgments

This work was financially supported by the National Key Technology Research and Development Program of the Ministry of Science and Technology (2013BAC11B00) and “Strategic Priority Research Program-Climate Change: Carbon Budget and Related Issues” of the Chinese Academy of Sciences, Grant No. XDA05010109, XDA05010110, XDA05010204 and the Natural Science Foundation of China (21343012).

Appendix A. Supplementary data

Supplementary data related to this article can be found at http://dx.doi.org/10.1016/j.jpowsour.2013.11.037.

References

[1] K.M. Yu, I. Curcic, J. Gabriel, S.C. Tsang, ChemSusChem 1 (2008) 893–899.
[2] B. Li, Y. Duan, D. Luebke, B. Morreale, Appl. Energy 102 (2013) 1439–1447.
[3] R. Steeneveldt, B. Berger, T.A. Torp, Chem. Eng. Res. Des. 84 (2006) 739–763.
[4] S. Chen, Z. Xue, D. Wang, W. Xiang, J. Power Sources 215 (2012) 89–98.
[5] W. Wang, S. Wang, X. Ma, J. Gong, Chem. Soc. Rev. 40 (2011) 3703–3727.
[6] G.A. Olah, Angew. Chem. Int. Ed. Engl. 44 (2005) 2636–2639.
[7] S.-i. Fujita, Catal. Today 45 (1998) 241–244.
[8] K. Klier, Adv. Catal. 31 (1982) 243–313.
[9] L.Z. Gao, C.T. Au, J. Catal. 189 (2000) 1–15.

[10] S. Natesakhawat, J.W. Lekse, J.P. Baltrus, P.R. Ohodnicki, B.H. Howard, X. Deng, C. Matranga, ACS Catal. 2 (2012) 1667–1676.
[11] J. Słoczyński, R. Grabowski, A. Kozłowska, P. Olszewski, M. Lachowska, J. Skrzypek, J. Stoch, Appl. Catal. A 249 (2003) 129–138.
[12] J. Sloczynski, R. Grabowski, P. Olszewski, A. Kozlowska, J. Stoch, M. Lachowska, J. Skrzypek, Appl. Catal. A 310 (2006) 127–137.
[13] M.S. Jingang Wu, Hirotaka Mabuse, Catal. Lett. 68 (2000) 55–58.
[14] X. Guo, D. Mao, G. Lu, S. Wang, G. Wu, J. Mol. Catal. A: Chem. 345 (2011) 60–68.
[15] L. Jia, J. Gao, W. Fang, Q. Li, Catal. Commun. 10 (2009) 2000–2003.
[16] L. Jia, J. Gao, W. Fang, Q. Li, J. Rare Earths 28 (2010) 747–751.
[17] M.A. .Peña, J.L.G. .Fierro, Chem. Rev. 101 (2001) 1981–2017.
[18] H. Zhong, R. Zeng, J. Serb. Chem. Soc. 71 (2006) 1049–1059.
[19] F. Riza, C. Ftikos, J. Eur. Ceram. Soc. 27 (2007) 571–573.
[20] L. Gao, G. Sun, S. Kawi, J. Solid State Chem. 181 (2008) 7–13.
[21] N. Tien-Thao, H. Alamdari, S. Kaliaguine, J. Solid State Chem. 181 (2008) 2006–2019.
[22] G. Valderrama, A. Kiennemann, M.R. Goldwasser, J. Power Sources 195 (2010) 1765–1771.
[23] G. Valderrama, C. Urbina de Navarro, M.R. Goldwasser, J. Power Sources 234 (2013) 31–37.
[24] Z.L. Yuan, L.N. Wang, J.H. Wang, S.X. Xia, P. Chen, Z.Y. Hou, X.M. Zheng, Appl. Catal. B: Environ. 101 (2011) 431.
[25] R.Q. Yang, X.C. .Yu, Y. Zhang, W.Z. Li, N. Tsubaki, Fuel 87 (2008) 443.
[26] R.D. Shannon, Acta Crystallogr. A 32 (1976) 751.
[27] N. Merino, B. Barbero, P. Grange, L. Cadus, J. Catal. 231 (2005) 232–244.
[28] Q.A. Islam, S. Nag, R.N. Basu, Mater. Res. Bull. 48 (2013) 3103–3107.
[29] V. Narayanan, K. de Buysser, E. Bruneel, I.v. Driessche, Materials 5 (2012) 364–376.
[30] S.S. Maluf, P.A.P. Nascente, C.R.M. Afonso, E.M. Assaf, Appl. Catal. A 413–414 (2012) 85–93.
[31] S.I. Fujita, M. Usui, N. Takezawa, J. Catal. 134 (1992) 220–225.
[32] F. Arena, G. Italiano, K. Barbera, G. Bonura, L. Spadaro, F. Frusteri, Catal. Today 143 (2009) 80–85.
[33] F. Arena, G. Italiano, K. Barbera, S. Bordiga, G. Bonura, L. Spadaro, F. Frusteri, Appl. Catal. A 350 (2008) 16–23.
[34] A.F. Lucrédio, G.T. Filho, E.M. Assaf, Appl. Surf. Sci. 255 (2009) 5851–5856.
[35] D.G. Cantrell, L.J. Gillie, A.F. Lee, K. Wilson, Appl. Catal. A 287 (2005) 183–190.
[36] B. Vijaya Kumar, R. Velchuri, G. Prasad, B. Sreedhar, K. Ravikumar, M. Vithal, Ceram. Int. 36 (2010) 1347–1355.
[37] F. Yan, Z.T. Liu, W.T. Liu, Phys. B 406 (2011) 2827–2833.
[38] X. Guo, D. Mao, G. Lu, S. Wang, G. Wu, J. Catal. 271 (2010) 178–185.
[39] P. Gao, F. Li, H. Zhan, F. Xiao, N. Zhao, W. Wei, L. Zhong, Y. Sun, J. Catal. 298 (2013) 51–60.
[40] L. Zhang, Y. Zhang, S. Chen, Appl. Catal. A 415–416 (2012) 118–123.
[41] H. Wilmer, J. Catal. 215 (2003) 188–198.
[42] K. Waugh, Solid State Ionics 168 (2004) 327–342.
[43] Y. Liu, K. Sun, H. Ma, X. Xu, X. Wang, Catal. Commun. 11 (2010) 880–883.
[44] D. Tichit, N. Das, B. Coq, R. Durand, Chem. Mater. 14 (2002) 1530–1538.
[45] Z.Q. Li, M. Meng, Y.Q. Zha, F.F. Dai, T.D. Hu, Z.Y. Hou, Y.N. Xie, Appl. Catal. B: Environ. 121–122 (2012) 65–74.
[46] K. Sutthiumporn, S. Kawi, Int. J. Hydrogen. Energy 36 (2011) 14435–14446.